

Special issue on *Sustainable Environmental Processes and Technologies*

PREPARATION AND CHARACTERIZATION OF MESOPOROUS CERIUM OXIDE FOR TOXIC AS(V) REMOVAL: PERFORMANCE AND MECHANISTIC STUDIES

Uttam Kumar SAHU^{1, 2}, Sandip MANDAL^{1, 2, 3}, Sumanta SAHU¹,
Narayan GOUDA⁴, Raj Kishore PATEL^{1*}

¹Department of Chemistry, National Institute of Technology, Rourkela, Odisha, India

²State Key Laboratory of Geohazard Prevention and Geoenvironment Protection
(Chengdu University of Technology), 1#, Dongsanlu, Erxianqiao, 610059 Chengdu, Sichuan, P. R. China

³School of Earth Sciences and Environmental Engineering, Gwangju Institute of Science and Technology (GIST),
Gwangju, Republic of Korea

⁴School of Applied Sciences, Department of Chemistry, Centurion University of Technology and Management,
761211 Odisha, India

Received 24 October 2020; accepted 16 November 2021

Highlights

- ▶ Mesoporous cerium oxide (MCO) had a good surface area of 191.97 m²/g.
- ▶ The MCO had a maximum adsorption capacity of 58.25 mg/g.
- ▶ The adsorption of As(V) was found to be pH sensitive.
- ▶ CO₃²⁻ and PO₄³⁻ ions affect the removal performance than Cl⁻, NO₃⁻ and SO₄²⁻.
- ▶ The MCO was found to be reusable for up to four cycles.

Abstract. In the present work, the adsorption of carcinogenic pentavalent arsenic (As(V)) from an aqueous solution was studied using mesoporous cerium oxide (MCO). The MCO was synthesized in the precipitation process and confirmed by FT-IR, SEM-EDX, XRD, and BET instrumental techniques. Batch adsorption showed that 95% of As(V) was removed in the optimum conditions of 0.60 g/L adsorbent dose, 10 mg/L initial concentration, time 30 min, and pH 3. Pseudo-second-order kinetics and the Langmuir isotherm model were fitted to the experimental data. The MCO had a high surface area of 191.97 m²/g and a maximum adsorption capacity of 58.25 mg/g at pH 3. MCO could be able to remove 88% and 82% in the first and second cycles after being desorbed with 0.1 M NaOH solution. The Zeta potential and FTIR studies suggested that electrostatic attraction and ligand exchange mechanisms were responsible for As(V) adsorption.

Keywords: mesoporous cerium oxide, As(V), adsorption, desorption and removal.

Introduction

The presence of arsenic in both surface and groundwater is mainly because of man-made and natural causes, specifically (a) uses of insecticides and pesticides (b) mining-related activities, (c) waste disposal (d) chemical products (e) wood preservation and (f) mobilization of natural arsenic on sediments (Kundu & Gupta, 2006; Shao et al., 2008). Arsenic is a semi-metal element mainly found as in two oxidation states “arsenite {As(III)} and arsenate {As(V)}”. Arsenic is tasteless, odorless, and found in water

in the form of H₂AsO₃⁻, HAsO₃²⁻, AsO₃³⁻, H₂AsO₄⁻, HAsO₄²⁻, and AsO₄³⁻. Additionally, As(III) have higher toxicity than As(V) because of electronic configuration and stability in water. As(V) is major species than As(III) in oxidizing environments, so more dominant in the natural water environment (Kim et al., 2004; Smedley & Kimbrough, 2002). The concentration of arsenic in drinking water should be less than 0.01 mg/L as prescribed by the World Health Organization (WHO) and the United States Environmental Protection Agency (USEPA) (Gerente et al., 2010). Frequent consumption of As(V) contained

*Corresponding author. E-mail: rkpatel@nitrrkl.ac.in

water brings major health-related difficulties e.g. Cancer in the liver, stomach, kidney, and skin (Benramdane et al., 1999).

Hence, the purification of As(V) is essential, and the available methods are ion exchange (Kim & Benjamin, 2004), coagulation-flocculation (Başkan et al., 2010), membrane filtration (Uddin et al., 2007), reverse osmosis (Pawlak et al., 2006), and adsorption (Mou et al., 2012). Compared to the methods reported in the literature, the adsorption process is suitable, efficient, and low cost respectively (Hu et al., 2020; Liang et al., 2021; Liu et al., 2021b). The process is operational at a small scale and can be utilized on a laboratory scale (Sahu et al., 2017). Metal oxide nanoparticles (iron oxide, zirconium oxide, manganese oxide, cerium oxide, titanium oxide, etc.), especially rare earth elements are considered to be an effective adsorbent material for their high specific surface area and specific selectivity towards arsenic, fluoride, and phosphate removal from water (Wu & Zhao, 2011). Among these, CeO₂ nanoparticles have gained visible attraction and use in various fields (UV-adsorbing agents, automotive catalytic converters, and gas sensors respectively (Chen et al., 2006; Zholobak et al., 2011). The cerium oxide nanoparticles are stable in acidic and basic conditions which can be helpful to increase the adsorption capacity of As(V). Again, the small ionic radius and higher surface hydroxyl groups of CeO₂ nanoparticles can potentially act as a good adsorbent for As(V) removal. However, the effectiveness of cerium oxide is limited because due to large agglomeration by electrostatic interactions which can significantly reduce the specific surface area (Wu et al., 2012). To overcome this limitation, recently mesoporous metal oxide nanoparticles have been prepared which have a high specific surface area, confined pore size, and stable pore volume due to interconnected frameworks with active pore surface (Wu & Zhao, 2011). To eliminate As(V) from water, previously used materials are mesoporous alumina (Kim et al., 2004), mesoporous carbon (Chen et al., 2007), and mesoporous mixed oxide (Zhang et al., 2013). However, these materials are having limitations with lower adsorption capacity and complex adsorption phenomena.

In this current study, mesoporous cerium oxide (MCO) is synthesized, characterized and used to examine the As(V) removal efficiency from an aqueous solution. The main motivation of this study is to know the effect of process parameters like dose, pH, contact time, initial concentration, adsorption efficiency, and reusability for As(V) removal. To understand the kinetics, isotherms and mechanism for As(V) on the MCO surface.

1. Materials and methods

1.1. Materials

All the chemicals used for the study were analytical and laboratory-grade. The cerium nitrate hexahydrate (Ce(NO₃)₃·6H₂O), sodium dihydrogen arsenate heptahydrate (NaH₂AsO₄·7H₂O), and cetyltrimethylammonium

bromide (CTAB (C₁₉H₄₂BrN)) were purchased from Sigma-Aldrich. Double distilled water was used for stock solution preparation and carrying in other studies.

1.2. Preparation of mesoporous cerium oxide (MCO)

To prepare mesoporous cerium oxide, the well-known surfactant CTAB was used as a soft template in the precipitation process (Sahu et al., 2016). 0.012 mol of Ce(NO₃)₃·6H₂O was dissolved in 40 mL ethanol and rapidly stirred for 15 min at ~200 rpm. In another beaker, 0.036 mol of CTAB was added in 100 mL water and both the solution were mixed with vigorous stirring at ~400 rpm. The surfactant was used to reduce the agglomeration of the metal salt with the formation of a micelle, which controls the growth of larger metal oxide particles formation. Then, NaOH was added to the above solution up to pH 9.05±0.2 with rapid stirring for 60 min, to completely precipitate the cerium species as their hydroxide. Then, the precipitate was washed several times with double deionized water and subsequently with ethanol. After washing completely the obtained samples were kept in an oven at 90 °C for 24 h. Then, it was again put in a furnace and dried at 300 °C for 3 h. The obtained materials were named MCO and kept in a sealed bottle. Cerium oxide (CO) was prepared by the same procedure but without the addition of CTAB and thermal treatment (300 °C).

1.3. Batch adsorption experiment

A 1000 mg/L of As(V) stock solution was prepared for batch adsorption studies and from which a complete series of different process parameters had been analyzed. First, a 50 mg MCO adsorbent was added to 100 mL of initial 10 mg/L As(V) solutions in a 250 mL bottle at pH 7 and shaken for 2 h in a rotary shaker with 300 rpm. After adsorption, the solution was centrifuge with 5000 rpm for 10 min, and left As(V) concentration was measured by atomic absorption spectroscopy (Elico SL 176, India). The percentage of removal (*R*) and uptake capacity (*q_e*) were analyzed by the followings equations:

$$R(\%) = \frac{(C_0 - C_e)}{C_0} \times 100; \quad (1)$$

$$q_e = \frac{(C_0 - C_e)}{w} \times v, \quad (2)$$

where: *R* and *q_e* are removal rate (%) and uptake capacity (mg/g), *C₀* and *C_e* are initial and equilibrium concentrations (mg/L), *v* is the volume of the solution (L) and *w* is the weight of the adsorbent (g), respectively.

1.4. Isotherm study

Effect of initial concentration was studied with 1–50 mg/L As(V) solutions under optimum condition and the obtained results were fitted with Langmuir and Freundlich isotherm model. The Langmuir isotherm explains the

monolayer adsorption on the homogenous surface, where the adsorption energy is the same for each binding site present on the adsorbent surface (Langmuir, 1916). But the Freundlich model explains the multilayer adsorption on the heterogeneous adsorbent surface, where the adsorption energy is different for the multiple binding sites on the adsorbent surface (Freundlich, 1906). The monolayer and multilayer adsorption were analyzed based on nonlinear Langmuir and Freundlich isotherms and can be expressed by the following equations:

$$q_e = \frac{q_m b C_e}{1 + b C_e}; \quad (3)$$

$$q_e = K_F C_e^{1/n}, \quad (4)$$

where: b (L/g) and K_F (mg/g) are Langmuir and Freundlich isotherm constant, and q_m is maximum adsorption capacity (mg/g), and n is a heterogeneity factor.

1.5. Kinetic study

The effect of contact time was studied from 0–60 min, to know the time-dependent analysis for As(V) removal by MCO. The results obtained from contact time were fitted to pseudo-first-order and pseudo-second-order models to know the adsorption kinetics for this experimental analysis. The pseudo-first-order model shows the physical adsorption process by van der Waals force of attraction between adsorbent and adsorbate. The pseudo-second-order model gives the information of the chemisorption process by sharing electrons or ligand exchange between adsorbent and adsorbate (Zhang et al., 2013). The nonlinear pseudo-first-order rate equation and pseudo-second-order rate equation was applied to know the adsorption kinetics were as follows:

$$q_t = q_e (1 - e^{-K_1 t}); \quad (5)$$

$$q_t = \frac{q_e^2 K_2 t}{1 + q_e k_2 t}, \quad (6)$$

where: q_t is uptake capacity at any time t (min), K_1 and K_2 are rate constants of pseudo-first-order adsorption (1/min) and second-order rate equation (g/mg·min) respectively.

1.6. pH, coexisting anions and desorption study

The As(V) removal was highly pH-dependent and effectiveness is achieved at optimal pH. Under optimum conditions of adsorbent dose 60 mg/L, initial concentration 10 mg/L, contact time 30 min, the solution pH (2–11) was maintained with 0.1 M HCl and 0.1 M NaOH solutions. The other common ions (Cl^- , NO_3^- , SO_4^{2-} , CO_3^{2-} and PO_4^{3-}) had also been tested on As(V) removal, where As(V) concentration was 10 mg/L while other ions concentrations were varied from 0–100 mg/L. The desorption experiments of As(V) on the adsorbent surface were performed with 0.1 M NaOH solutions. The desorbed

adsorbent was used for up to four consecutive cycles to calculate its performance for regeneration ability and feasibility in practical applications.

1.7. Characterization of the adsorbent

The wide-angle XRD was used to know the crystallization properties of the CO and MCO materials. The Philips X'pert X-ray diffractometer model PW 1830 (Almelo, Netherlands) XRD instruments are used with Cu $K\alpha$ radiation (35 kV and 30 mA) over in the range of 10–70° with a scanning rate of 3° per min. The morphology and surface elements of CO and MCO were analyzed by field emission scanning electron microscopy (Fe-SEM) and EDX (JEOL, JSM-6480 LV analyzer). The atomic-level morphology and particle size of MCO are studied by using TEM and HRTEM (JEOL 3010, Japan) analysis. The mesoporosity of the materials is confirmed with BET analysis, the detailed specific surface area, pore size, and volume of CO and MCO is studied with BET analyzer (Quanta chrome AUTOSORB-1, Boynton Beach, Florida). Perkin-Elmer- RX-I, Fourier Transform Infrared Spectroscopy (FTIR) instrument is used to detect the functional groups present on CO and MCO (before and after As(V) adsorption) surface. The materials were prepared with KBr pellets with a pressure of 6 tons. The surface charges of MCO before and after adsorption were calculated with a zeta potential analyzer (Nano Z, Malvern, UK).

2. Result and discussion

2.1. Characterization of the adsorbent

2.1.1. Morphology of the adsorbent

The detailed morphological analysis of CO and MCO is represented in Figure 1. From Figure 1a, the CO had different size particles without any systematic distributions. Figure 1b shows that the MCO prepared with CTAB surfactant had comparatively large but in uniform shape and was present regularly. From Figure 1c, it was observed that the surface morphology of MCO was completely changed after the adsorption. Very large aggregation was seen due to adsorption of As(V) on the MCO surface. Further confirmation was obtained from the EDX image (Figure 1d) where Ce, O, and As were present on the materials which confirmed As(V) was adsorbed on the MCO surface. The internal structure of MCO was identified from the TEM image as shown in Figure 1e. Very small size particles were present on MCO. The HRTEM image (Figure 1f) of MCO clarified that the small size particles with an average diameter of 6–8 nm.

2.1.2. XRD study

Figure 2 represents the XRD patterns of CO and MCO. The major peak at 28.5° (111), 33.1° (200), 47.9° (220) 56.8° (311), and 59.3° (222) were matched with all five major peaks of CeO_2 with JCPDS file 34-039435 (Sahu et al., 2016). The XRD peaks of MCO were the same as

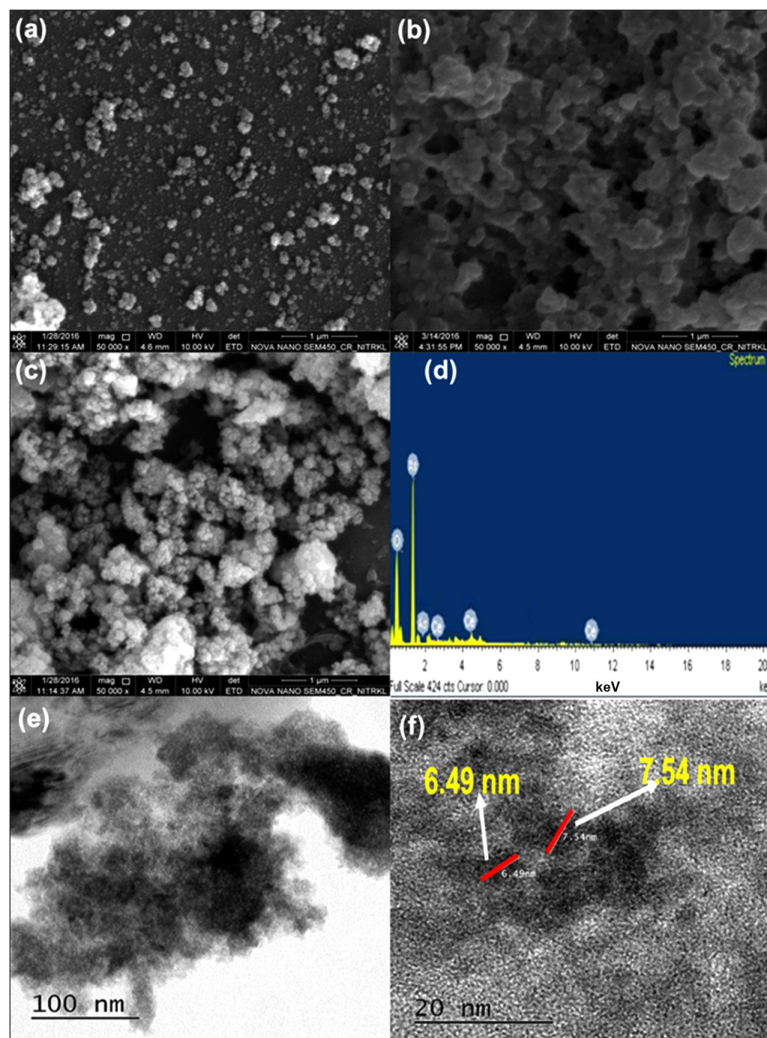


Figure 1. FESEM images of CO (a), MCO (b, c) before and after As(V) adsorption, EDX of As(V) loaded MCO (d), TEM and HRTEM of MCO (e, f)

CO but the peaks intensity of mesoporous CeO_2 was decreased. This might have been caused by interconnectivity between the mesoporous systems results in the formation of lower symmetry (Chen et al., 2014; Selvi et al., 2014).

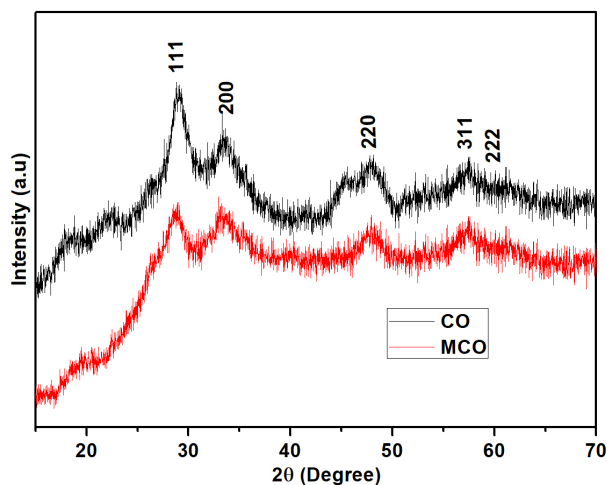


Figure 2. XRD patterns of CO and MCO

2.1.3. Specific surface area

A nitrogen adsorption-desorption isotherms study was done to know the mesoporosity of the adsorbent. The CO formed a type III isotherm which is indicated in Figure 3a. As different sizes of particles were present on the CO and it was not able to provide a suitable assessment of pore size distribution as shown in Figure 3b. The specific surface area of the CO was not high and was found to be $78.39 \text{ m}^2/\text{g}$. The average pore size and pore volume of CO were found to be 3.5 nm and 0.062 cm^3 , respectively. But in the case of the MCO (Figure 3c), a type IV isotherm was seen with the hysteresis loop at P/P_0 in the range of 0.4 to 0.95, which is the characteristic of a mesoporous material (Sahu et al., 2017). The specific surface area increased to $191.97 \text{ m}^2/\text{g}$, which is higher as compared to the previously reported literature (Basu & Ghosh, 2013; Chen et al., 2014). The pore size and pore volume of MCO were found to be 4.9 nm (Figure 3d) and 0.164 cm^3 respectively. The significant increase in specific surface area and pore size of MCO leads to better advantages for the removal of As(V) with the high specific surface area.

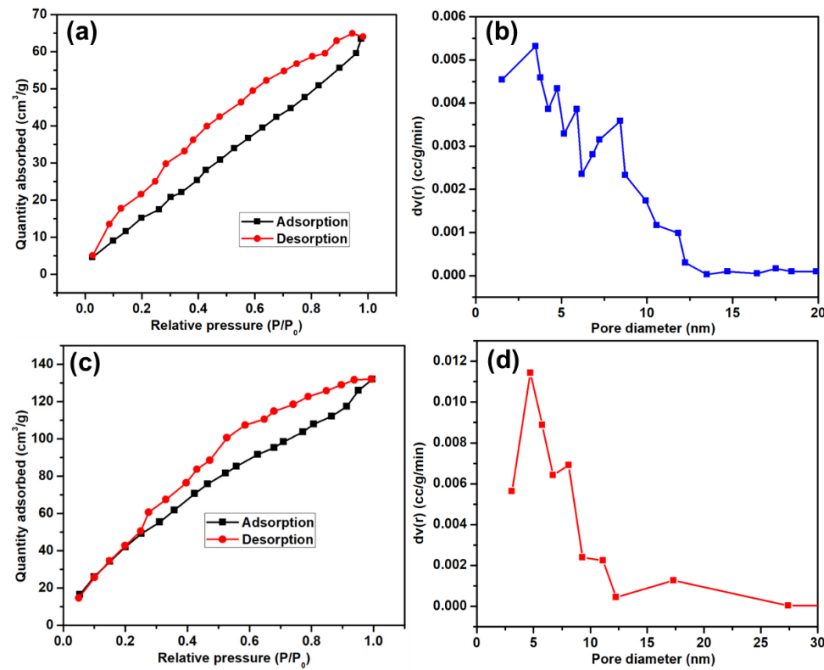


Figure 3. Adsorption-desorption isotherm and pore diameter of CO (a, b) and MCO (c, d)

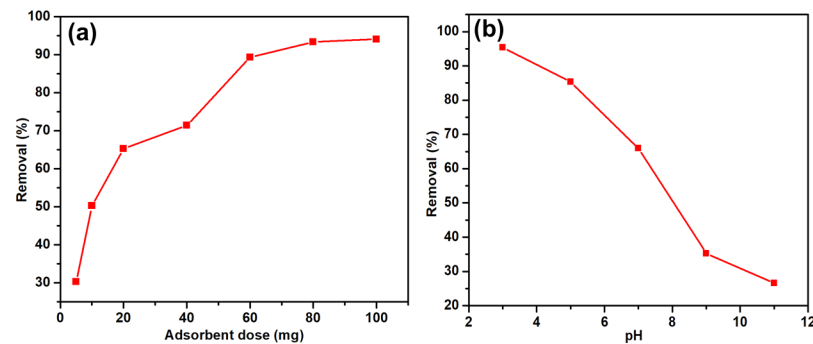


Figure 4. Effect of adsorbent dose (a) and pH (b) on As(V) removal

2.2. Effect of adsorbent dose and pH

The adsorption capacity and real-time practical applications are highly dependent on the amount of adsorbent used in the removal process. Here adsorption was performed with 10 mg/L initial As(V) solutions with different amounts of adsorbent dose from 10–60 mg. From Figure 4a, it was predicted that a very less amount of MCO was high enough to remove As(V) from the contaminated solutions. About 90% of As(V) was removed with an adsorbent dose of 60 mg and after that, it became slightly increase up to 100 mg. Initially, the adsorbate is attached to the surface and diffuse on the pore of the adsorbent and after that, no further diffusion takes place which leads to no additional adsorption take place on the adsorbent surface (Sahu et al., 2019). Hence, 60 mg was taken as an optimum adsorbent dose in this removal study.

Figure 4b shows the pH effect on As(V) removal by MCO nanoparticles. The removal was 95% at pH 3 and significantly decreased to 26% at pH 11. These intense results were at lower and higher pH, mainly for the surface

charge of the adsorbent and As(V) speciation in different pH (Guan et al., 2009). At lower pH from 2–6, the MCO surface was highly positively charged due to H⁺ ions protonation and at the same time As(V) ions existed in H₂AsO₄⁻ forms. Hence electrostatic attraction occurred rapidly and the maximum amount of As(V) was removed in this lower pH range. But with an increase in pH, the –OH ions concentrations increased and the adsorbent surface positivity decreased and at higher pH, As(V) exists in HAsO₄²⁻ and AsO₄³⁻, hence electrostatic repulsion occurred between MCO surface and arsenic species which brings a drastic decrease in removal rate. The optimum pH was obtained for this experimental study was 3.

2.3. Effect of contact time and adsorption kinetics

Figure 5 shows the effect of contact time on the removal of As(V) by MCO. This time-dependent study had been performed with 60 mg adsorbent, 10 mg/L As(V) solution, pH 3, and times vary from 0–60 min. The removal rate was maximum and equilibrium reached 30 min and after

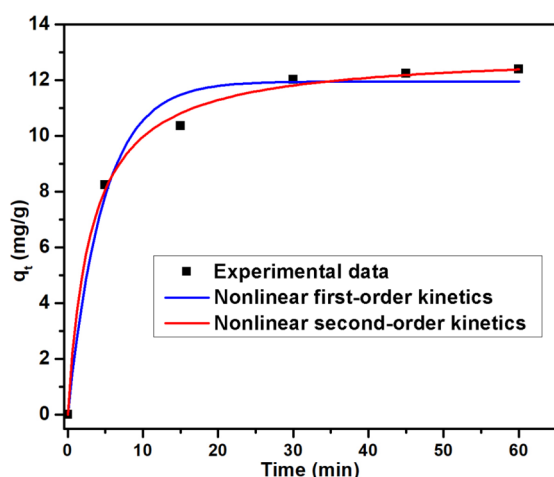


Figure 5. Nonlinear first-orders and second-order kinetics plot

that, it remains constant. Initially, the As(V) was rapidly adsorbed on the pore cavity and outer surface of MCO, and with further increase in time, its adsorption rate became slow. The nonlinear curves of both first and second-order models were fitted to the experimental data and the respective kinetics model parameters are presented in Table 1. The second-order model was better fitted to the experimental data and had higher correlation coefficients ($R^2 = 0.99$) than those of the first-order model ($R^2 = 0.98$). In literature, similar kinetic model results have been reported for the analysis of adsorption kinetic data of various pollutants in different adsorbent-adsorbate systems

Table 1. Kinetic parameters and correlation coefficients (R^2) for pseudo-first-order and pseudo-second-order kinetic models

Pseudo-first-order			Pseudo-second-order		
q_e (mg/g)	K_1 (1/min)	R^2	q_e (mg/g)	K_2 (g/mg·min)	R^2
11.96	0.21	0.98	13.01	0.02	0.99

Table 2. Langmuir and Freundlich isotherm parameters for As(V) adsorption

Langmuir isotherm			Freundlich isotherm		
q_m (mg/g)	b (L/g)	R^2	K_f (mg/g)	n	R^2
58.25	0.151	0.94	12.32	3.16	0.87

Table 3. Comparison study of adsorption capacity of As(V) with other adsorbents

Adsorbents	Experimental conditions	q_m (mg/g)	References
Granular Fe–Ce oxide	Temperature 25 °C, pH 5, time 48 h, concentration 10 mg/L	18.20	(Zhang et al., 2010)
Binary oxide of iron and silicon	Temperature, pH 3, time 15 h, concentration 50 mg/L	20.70	(Mahmood et al., 2012)
Ce-Fe bimetal mixed oxide	Temperature 25 °C, pH 3, time 60 min, concentration 10 mg/L	32.12	(Sahu et al., 2016)
Mesoporous iron-manganese bimetal oxide	Temperature 25 °C, pH 3, time 24 h, concentration 10 mg/L	35.35	(Wen et al., 2014)
iron(III)–cerium(IV) oxide	Temperature 30 °C, pH 7, time 60 min, concentration 4.5 mg/L	55.51	(Basu et al., 2013)
Mesoporous cerium oxide	Temperature 25 °C, pH 3, time 30 min, concentration 10 mg/L	58.25	Present study

(Duman et al., 2015, 2020, 2016b). The fitting of pseudo-second-order kinetics explained that the As(V) adsorption on the MCO surface was a chemisorption process, which was happened due to the exchange of electrons and valence forces between As(V) and MCO (Li et al., 2012).

2.4. Effect of initial concentration and adsorption isotherm

The effect of initial concentration (1–50 mg/L) studies was done with 60 mg adsorbent dose, contact time 30 min, and pH 3. From Figure 6, it was observed that at a lower concentration maximum amount of As(V) had been adsorbed continuously increased up to 10 mg/L and after

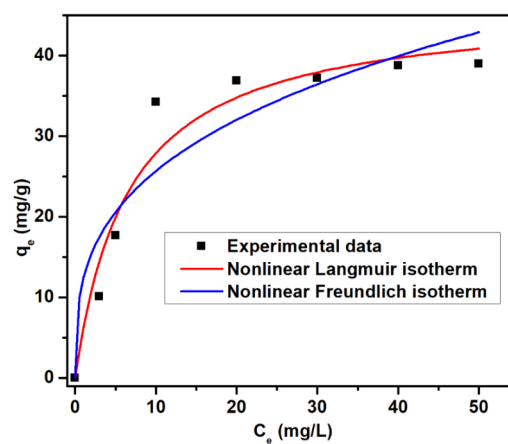


Figure 6. Nonlinear Langmuir and Freundlich adsorption isotherm plot

that it became constant. At lower concentrations, the As(V) ions were less but greater binding sites on the surface of the adsorbent which brings very good results in the removal rate. But at higher concentrations, the availability of active binding sites was very less compared to the number of As(V) molecules, which gave less rate of removal. Both the Langmuir and Freundlich isotherm models were fitted with the As(V) removal data with a different initial concentration in optimizing conditions. The fitting results obtained from the isotherm parameter are concise in Table 2. It was obtained that the Langmuir isotherm model suitable agreed with experimental data with $R^2 = 0.94$ than the Freundlich isotherm model with $R^2 = 0.87$. Again, the value of R_L was 0.398, found in-between 0 to 1, which again confirmed that the Langmuir adsorption process was favorable for As(V) removal on the MCO surface. The obtained isotherm result is consistent with the literature (Duman et al., 2019, 2016a). The adsorption capacities for As(V) with previously reported metal oxides are presented in Table 3. The details of comparison studies with other adsorbents are explained in the supporting information file.

2.5. Effect of coexisting anion

Figure 7 shows the effects of Cl^- , NO_3^- , SO_4^{2-} , CO_3^{2-} and PO_4^{3-} ions on the removal of As(V) by MCO. The experimental analysis showed that order of: $\text{PO}_4^{3-} > \text{CO}_3^{2-} > \text{SO}_4^{2-} > \text{NO}_3^- > \text{Cl}^-$ for As(V) removal. The effects of Cl^- , NO_3^- and SO_4^{2-} were very less due to its lower competition to the binding sites of MCO as compared to As(V) (Guan et al., 2009). In the presence of CO_3^{2-} , the successive decrease was seen in As(V) removal rate as carbonate forms arseno-carbonate complexes which result in additional uptake of carbonate. Same time, PO_4^{3-} and arsenate are present in the same group in the periodic table and highly competitive with each other with the binding sites on the MCO surface and results in a lower removal rate for As(V) (Tang & Zhang, 2016).

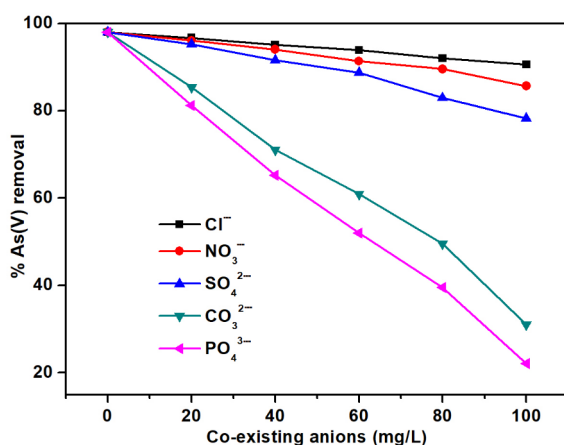


Figure 7. Effect of coexisting anions on As(V) removal

2.6. Desorption and reusability study

A desorption study was conducted with 0.1 M NaOH solution for further use of MCO to remove As(V) from actual wastewater. Figure 8 shows the repeated use of desorbed MCO for four cycles and the As(V) removal rate was decreased to 51% in the fourth cycle. This decrease was mainly due to a decrease in active pores or degradation of active sites of MCO. The Ce ions leaching studies had also been done to avoid additional heavy metal pollutions in the water. We observed that the concentration of Ce ions in the solutions was 5.6 mg/L and 2.3 mg/L in the fresh and fourth cycles. Hence, we found that this many Ce ions in water don't bring any problems for living organisms.

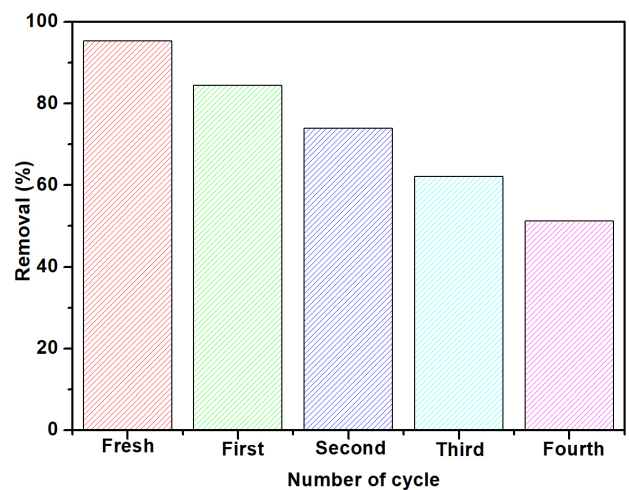


Figure 8. The adsorption capacity of MCO at different cycles

2.7. Adsorption mechanism

FTIR, zeta potential measurements and Fe-SEM were considered for establishing the mechanism of adsorption onto MCO. Clear observation was recorded from Figure 1d, for arsenic adsorption from EDX data onto MCO surface, the morphology after adsorption is found to be altered from the before adsorption case (Figure 1c). Figure 9 depicts the isoelectric point of the MCO before and after As(V) adsorption. The MCO exhibited a strongly positively charged

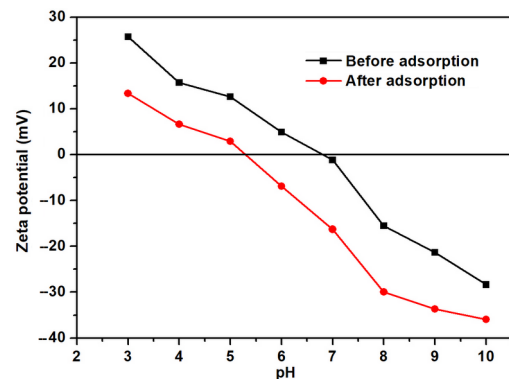


Figure 9. Zeta potential study of MCO before and after adsorption

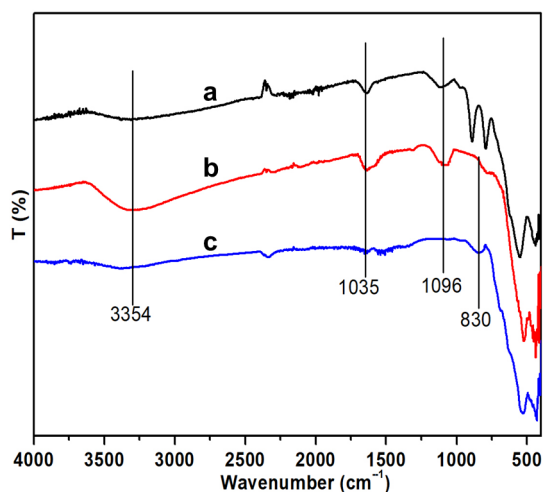


Figure 10. FTIR spectra of CO (a), MCO (b) and As(V) loaded MCO (c)

surface at lower pH, and surface positivity declined as pH increased, becoming substantially negative at pH 11. After As(V) adsorption, the isoelectric point of MCO was ~ 6.7 , while it was ~ 5.3 previously. A negative charge on As(V) species (H_2AsO_4^-) causes the surface's isoelectric point to change following adsorption. Additionally, due to electrostatic attraction, the As(V) was adsorbed on MCO's surface, and the isoelectric point decreased from ~ 6.7 to 5.3. Previously same types of observation for other adsorbent have been seen in other adsorbents (Dai et al., 2019; Huo et al., 2021; Liu et al., 2021a; Zhu et al., 2021). For CO and MCO, Figure 10 shows both their pre- and post-adsorption spectrums. Both the $\sim\text{OH}$ bending and stretching vibrations had maxima at 3354 cm^{-1} and 1635 cm^{-1} , which corresponded to the corresponding two main peaks. Ce-OH vibrations were detected at 1096 cm^{-1} , causing the bend (Nakamoto, 1978). The two sharp bands around at 870 and 860 cm^{-1} were for Ce-O-Ce vibrations (Basu & Ghosh, 2013) and the bend at 534 cm^{-1} was for

the metal-oxygen bond (Ce-O). When MCO was bent, the vibrations of $\sim\text{OH}$ groups stretched and bent at high intensities, making them more suited for As(V) removal. When MCO was exposed to As(V) adsorption, however, numerous modifications were observed. The vibration bend at 1096 cm^{-1} Ce-OH vibration was fully removed with the formation of a new bend at 830 cm^{-1} , which is the bend for the Ce-O-As stretching vibration bond (Ren et al., 2011). Hence, the Ce-OH groups on the MCO surface were substituted by As(V) (H_2AsO_4^-) anions. There were also changes in the $\sim\text{OH}$ vibration bends at 3354 and 1635 cm^{-1} following adsorption of As(V). Adsorption of As(V) by $\sim\text{OH}$ groups on MCO surface was determined via ligand exchange processes. A similar observation was previously observed by other researchers (Basu et al., 2013; Chen et al., 2013). Aqueous As(V) was removed from the solution via ligand exchange and electrostatic attraction, as shown by the zeta potential measurements as well as infrared spectroscopy (FTIR). The proposed adsorption mechanism was presented in Figure 11.

Conclusions

The results obtained from the above have drawn several conclusions. Start with, the composite has a large number of uniformly distributed mesopores which increase the surface area ($191.97\text{ m}^2/\text{g}$) of MCO, provides a higher number of the binding site to catch As(V) ions. In addition, MCO has a good adsorption capacity of 59.32 mg/g at a contact time of 30 min, which also provides information that the adsorption process is complete in very little time with good removal accuracy. Furthermore, the MCO could be applied up to longer cycles (52% removed in 4th cycles) any problem (in presence of other ions also able to remove arsenic). The adsorption of As(V) on the MCO surface was confirmed by FTIR, Zeta potential, and SEM-EDX studies. Lastly, the monolayer and chemisorption adsorption process happen which will increase the

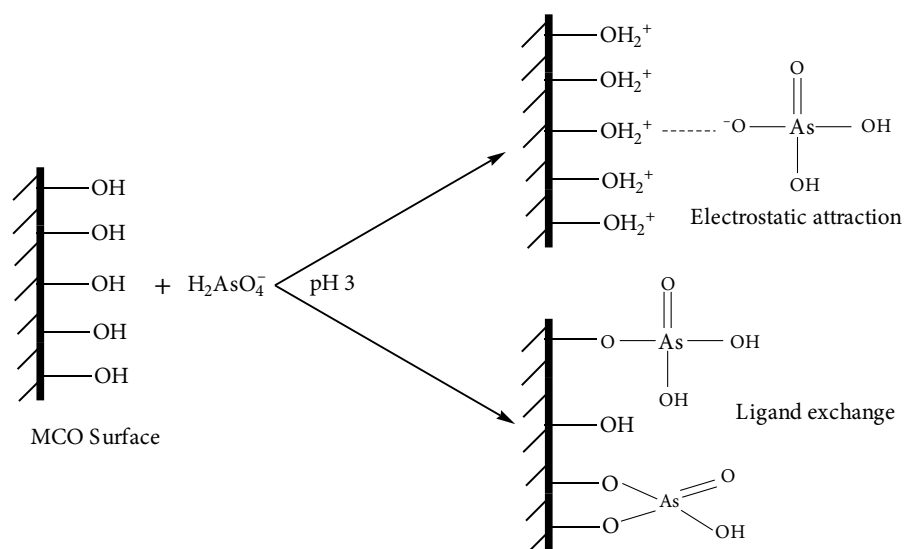


Figure 11. Proposed mechanism of the adsorption of As(V) on MCO surface

efficiency of the material in practical application in the arsenic-contaminated area.

Acknowledgements

The authors are also highly thankful to the National Institute of Technology, Rourkela for providing the instrumental facilities.

References

- Başkan, M. B., Pala, A., & Türkman, A. (2010). Arsenate removal by coagulation using iron salts and organic polymers. *Ekoloji*, 74(19), 69–76. <https://doi.org/10.5053/ekoloji.2010.7410>
- Basu, T., & Ghosh, U. C. (2013). Nano-structured iron(III)-cerium(IV) mixed oxide: Synthesis, characterization and arsenic sorption kinetics in the presence of co-existing ions aiming to apply for high arsenic groundwater treatment. *Applied Surface Science*, 283, 471–481. <https://doi.org/10.1016/j.apsusc.2013.06.132>
- Basu, T., Nandi, D., Sen, P., & Chand, U. (2013). Equilibrium modeling of As (III, V) sorption in the absence / presence of some groundwater occurring ions by iron (III)– cerium (IV) oxide nanoparticle agglomerates: A mechanistic approach of surface interaction. *Chemical Engineering Journal*, 228, 665–678. <https://doi.org/10.1016/j.cej.2013.05.037>
- Benramdane, L., Accominotti, M., Fanton, L., Malicier, D., & Vallon, J. J. (1999). Arsenic speciation in human organs following fatal arsenic trioxide poisoning—A case report. *Clinical Chemistry*, 45(2), 301–306. <https://doi.org/10.1093/clinchem/45.2.301>
- Chen, B., Zhu, Z., Hong, J., Wen, Z., Ma, J., Qiu, Y., & Chen, J. (2014). Nanocasted synthesis of ordered mesoporous cerium iron mixed oxide and its excellent performances for As(v) and Cr(vi) removal from aqueous solutions. *Dalton Transactions*, 43, 10767–10777. <https://doi.org/10.1039/C4DT01101E>
- Chen, Bo, Zhu, Z., Guo, Y., Qiu, Y., & Zhao, J. (2013). Facile synthesis of mesoporous Ce-Fe bimetal oxide and its enhanced adsorption of arsenate from aqueous solutions. *Journal of Colloid and Interface Science*, 398, 142–151. <https://doi.org/10.1016/j.jcis.2013.02.004>
- Chen, J., Patil, S., Seal, S., & McGinnis, J. F. (2006). Rare earth nanoparticles prevent retinal degeneration induced by intracellular peroxides. *Nature Nanotechnology*, 1, 142–150. <https://doi.org/10.1038/nnano.2006.91>
- Chen, W., Parette, R., Zou, J., Cannon, F. S., & Dempsey, B. A. (2007). Arsenic removal by iron-modified activated carbon. *Water Research*, 41, 1851–1858. <https://doi.org/10.1016/j.watres.2007.01.052>
- Dai, S., Wang, N., Qi, C., Wang, X., Ma, Y., Yang, L., Liu, X., Huang, Q., Nie, C., Hu, B., & Wang, X. (2019). Preparation of core-shell structure Fe₃O₄@C/MnO₂ nanoparticles for efficient elimination of U(VI) and Eu(III) ions. *Science of the Total Environment*, 685, 196–199. <https://doi.org/10.1016/j.scitotenv.2019.06.292>
- Duman, O., Özcan, C., Polat, T. G., & Tunç, S. (2019). Carbon nanotube-based magnetic and non-magnetic adsorbents for the high-efficiency removal of diquat dibromide herbicide from waterwater: OMWCNT, OMWCNT-Fe₃O₄ and OMWCNT-κ-carrageenan-Fe₃O₄ nanocomposites. *Environmental Pollution*, 244, 723–732. <https://doi.org/10.1016/j.envpol.2018.10.071>
- Duman, O., Polat, T. G., Diker, C. Ö., & Tunç, S. (2020). Agar/κ-carrageenan composite hydrogel adsorbent for the removal of Methylene Blue from water. *International Journal of Biological Macromolecules*, 160, 823–835. <https://doi.org/10.1016/j.ijbiomac.2020.05.191>
- Duman, O., Tunç, S., & Gürkan Polat, T. (2015). Adsorptive removal of triarylmethane dye (Basic Red 9) from aqueous solution by sepiolite as effective and low-cost adsorbent. *Microporous and Mesoporous Materials*, 210, 176–184. <https://doi.org/10.1016/j.micromeso.2015.02.040>
- Duman, O., Tunç, S., Bozoğlan, B. K., & Polat, T. G. (2016a). Removal of triphenylmethane and reactive azo dyes from aqueous solution by magnetic carbon nanotube-κ-carrageenan-Fe₃O₄ nanocomposite. *Journal of Alloys and Compounds*, 687, 370–383. <https://doi.org/10.1016/j.jallcom.2016.06.160>
- Duman, O., Tunç, S., Polat, T. G., & Bozoğlan, B. K. (2016b). Synthesis of magnetic oxidized multiwalled carbon nanotube-κ-carrageenan-Fe₃O₄ nanocomposite adsorbent and its application in cationic Methylene Blue dye adsorption. *Carbohydrate Polymers*, 147, 79–88. <https://doi.org/10.1016/j.carbpol.2016.03.099>
- Freundlich, H. (1906). User die adsorption in losungen [Adsorption in solution]. *The Journal of Physical Chemistry*, 57, 384–470. <https://doi.org/10.1515/zpch-1907-5723>
- Gerente, C., Andres, Y., McKay, G., & Le Cloirec, P. (2010). Removal of arsenic(V) onto chitosan: From sorption mechanism explanation to dynamic water treatment process. *Chemical Engineering Journal*, 158, 593–598. <https://doi.org/10.1016/j.cej.2010.02.005>
- Guan, X., Dong, H., Ma, J., & Jiang, L. (2009). Removal of arsenic from water: Effects of competing anions on As(III) removal in KMnO₄-Fe(II) process. *Water Research*, 43, 3891–3899. <https://doi.org/10.1016/j.watres.2009.06.008>
- Hu, B., Ai, Y., Jin, J., Hayat, T., Alsaedi, A., Zhuang, L., & Wang, X. (2020). Efficient elimination of organic and inorganic pollutants by biochar and biochar-based materials. *Biochar*, 2, 47–64. <https://doi.org/10.1007/s42773-020-00044-4>
- Huo, L., Zhao, S., Shi, B., Wang, H., & He, S. (2021). Bacterial community change and antibiotic resistance promotion after exposure to sulfadiazine and the role of UV/H₂O₂-GAC treatment. *Chemosphere*, 283, 131214. <https://doi.org/10.1016/j.chemosphere.2021.131214>
- Kim, J., & Benjamin, M. M. (2004). Modeling a novel ion exchange process for arsenic and nitrate removal. *Water Research*, 38, 2053–2062. <https://doi.org/10.1016/j.watres.2004.01.012>
- Kim, Y., Kim, C., Choi, I., Rengaraj, S., & Yi, J. (2004). Arsenic removal using mesoporous alumina prepared via a templating method. *Environmental Science & Technology*, 38, 924–931. <https://doi.org/10.1021/es0346431>
- Kundu, S., & Gupta, A. K. (2006). Adsorptive removal of As(III) from aqueous solution using iron oxide coated cement (IOCC): Evaluation of kinetic, equilibrium and thermodynamic models. *Separation and Purification Technology*, 51, 165–172. <https://doi.org/10.1016/j.seppur.2006.01.007>
- Langmuir, I. (1916). The constitution and fundamental properties of solids and liquids. *Journal of American Chemical Society*, 38, 2221–2295. <https://doi.org/10.1021/ja02268a002>
- Li, R., Li, Q., Gao, S., & Shang, J. K. (2012). Exceptional arsenic adsorption performance of hydrous cerium oxide nanoparticles: Part A. Adsorption capacity and mechanism. *Chemical Engineering Journal*, 185–186, 127–135. <https://doi.org/10.1016/j.cej.2012.01.061>
- Liang, L., Xi, F., Tan, W., Meng, X., Hu, B., & Wang, X. (2021). Review of organic and inorganic pollutants removal by biochar and biochar-based composites. *Biochar*, 3(3), 255–281. <https://doi.org/10.1007/s42773-021-00101-6>

- Liu, F., Hua, S., Wang, C., Qiu, M., Jin, L., & Hu, B. (2021a). Adsorption and reduction of Cr(VI) from aqueous solution using cost-effective caffeic acid functionalized corn starch. *Chemosphere*, 279, 130539. <https://doi.org/10.1016/j.chemosphere.2021.130539>
- Liu, X., Pang, H., Liu, X., Li, Q., Zhang, N., Mao, L., Qiu, M., Hu, B., Yang, H., & Wang, X. (2021b). Orderly porous covalent organic frameworks-based materials: Superior adsorbents for pollutants removal from aqueous solutions. *The Innovation*, 2(1), 100076. <https://doi.org/10.1016/j.xinn.2021.100076>
- Mahmood, T., Din, S. U., Naeem, A., Mustafa, S., Waseem, M., & Hamayun, M. (2012). Adsorption of arsenate from aqueous solution on binary mixed oxide of iron and silicon. *Chemical Engineering Journal*, 192, 90–98. <https://doi.org/10.1016/j.cej.2012.03.048>
- Mou, F., Guan, J., Ma, H., Xu, L., & Shi, W. (2012). Magnetic iron oxide chestnutlike hierarchical nanostructures: Preparation and their excellent arsenic removal capabilities. *ACS Applied Materials and Interfaces*, 4, 3987–3993. <https://doi.org/10.1021/am300814q>
- Nakamoto, K. (1978). *Infrared and raman spectra of inorganic and coordination compounds* (3rd ed.). John Wiley.
- Pawlak, Z., Zak, S., & Zablocki, L. (2006). Removal of hazardous metals from groundwater by reverse osmosis. *Polish Journal of Environmental Studies*, 15(4), 579–583.
- Ren, Z., Zhang, G., & Chen, P. J. (2011). Adsorptive removal of arsenic from water by an iron-zirconium binary oxide adsorbent. *Journal of Colloid and Interface Science*, 358, 230–237. <https://doi.org/10.1016/j.jcis.2011.01.013>
- Sahu, U. K., Sahu, M. K., Mohapatra, S. S., & Patel, R. K. (2016). Removal of As(V) from aqueous solution by Ce-Fe bimetal mixed oxide. *Journal of Environmental Chemical Engineering*, 4, 2892–2899. <https://doi.org/10.1016/j.jece.2016.05.041>
- Sahu, U. K., Sahu, S., Mahapatra, S. S., & Patel, R. K. (2017). Cigarette soot activated carbon modified with Fe₃O₄ nanoparticles as an effective adsorbent for As(III) and As(V): Material preparation, characterization and adsorption mechanism study. *Journal of Molecular Liquids*, 243, 395–405. <https://doi.org/10.1016/j.molliq.2017.08.055>
- Sahu, U. K., Sahu, S., Mahapatra, S. S., & Patel, R. K. (2019). Synthesis and characterization of magnetic bio-adsorbent developed from Aegle marmelos leaves for removal of As(V) from aqueous solutions. *Environmental Science and Pollution Research*, 26, 946–958. <https://doi.org/10.1007/s11356-018-3643-1>
- Selvi, N., Padmanathan, N., Dinakaran, K., & Sankar, S. (2014). Effect of ZnO, SiO₂ dual shells on CeO₂ hybrid core-shell nanostructures and their structural, optical and magnetic properties. *RSC Advances*, 4, 55745–55751. <https://doi.org/10.1039/C4RA07705A>
- Shao, W., Li, X., Cao, Q., Luo, F., Li, J., & Du, Y. (2008). Adsorption of arsenate and arsenite anions from aqueous medium by using metal(III)-loaded amberlite resins. *Hydrometallurgy*, 91, 138–143. <https://doi.org/10.1016/j.hydromet.2008.01.005>
- Smedley, P. L., & Kinniburgh, D. G. (2002). A review of the source, behaviour and distribution of arsenic in natural waters. *Applied Geochemistry*, 17, 517–568. [https://doi.org/10.1016/S0883-2927\(02\)00018-5](https://doi.org/10.1016/S0883-2927(02)00018-5)
- Tang, D., & Zhang, G. (2016). Efficient removal of fluoride by hierarchical Ce-Fe bimetal oxides adsorbent: Thermodynamics, kinetics and mechanism. *Chemical Engineering Journal*, 283, 721–729. <https://doi.org/10.1016/j.cej.2015.08.019>
- Uddin, M. T., Mozumder, M. S. I., Islam, M. A., Deowan, S. A., & Hoinkis, J. (2007). Nanofiltration membrane process for the removal of arsenic from drinking water. *Chemical Engineering & Technology*, 30(9), 1248–1254. <https://doi.org/10.1002/ceat.200700169>
- Wen, Z., Dai, C., Zhu, Y., & Zhang, Y. (2014). Arsenate removal from aqueous solutions using magnetic mesoporous iron manganese bimetal. *RSC Advances*, 5, 4058–4068. <https://doi.org/10.1039/C4RA09746G>
- Wu, Z., & Zhao, D. (2011). Ordered mesoporous materials as adsorbents. *Chemical Communications*, 47, 3332–3338. <https://doi.org/10.1039/c0cc04909c>
- Wu, Z., Li, W., Webley, P. A., & Zhao, D. (2012). General and controllable synthesis of novel mesoporous magnetic iron oxide@carbon encapsulates for efficient arsenic removal. *Advanced Materials*, 24, 485–491. <https://doi.org/10.1002/adma.201103789>
- Zhang, G., Ren, Z., Zhang, X., & Chen, J. (2013). Nanostructured iron(III)-copper(II) binary oxide: A novel adsorbent for enhanced arsenic removal from aqueous solutions. *Water Research*, 47, 4022–4031. <https://doi.org/10.1016/j.watres.2012.11.059>
- Zhang, Y., Dou, X., Zhao, B., Yang, M., Takayama, T., & Kato, S. (2010). Removal of arsenic by a granular Fe-Ce oxide adsorbent: Fabrication conditions and performance. *Chemical Engineering Journal*, 162, 164–170. <https://doi.org/10.1016/j.cej.2010.05.021>
- Zholobak, N. M., Ivanov, V. K., Shcherbakov, A. B., Shaporov, A. S., Polezhaeva, O. S., Baranchikov, A. Y., Spivak, N. Y., & Tretyakov, Y. D. (2011). UV-shielding property, photocatalytic activity and photocytotoxicity of ceria colloid solutions. *Journal of Photochemistry and Photobiology B: Biology*, 102, 32–38. <https://doi.org/10.1016/j.jphotobiol.2010.09.002>
- Zhu, Y., He, X., Xu, J., Fu, Z., Wu, S., Ni, J., & Hu, B. (2021). Insight into efficient removal of Cr(VI) by magnetite immobilized with *Lysinibacillus* sp. JLT12: Mechanism and performance. *Chemosphere*, 262, 127901. <https://doi.org/10.1016/j.chemosphere.2020.127901>